Ionics (2019) 25:3461–3471
https://doi.org/10.1007/s11581-019-02895-9

ORIGINAL PAPER

Antimicrobial properties of poly(propylene) carbonate/Ag nanoparticle-modified tamarind seed polysaccharide with composite films

Indira Devi M.P.[1] · Nallamuthu N.[1] · Rajini N.[2] · Senthil Muthu Kumar T.[2,3] · Suchart Siengchin[3] · Varada Rajulu A.[4] · Hariram N.[5]

Received: 4 December 2018 / Revised: 5 January 2019 / Accepted: 25 January 2019 / Published online: 12 February 2019

Abstract

Completely biodegradable poly(propylene)carbonate-based composite films with 10 wt.% of tamarind seed polysaccharide (TSP) as filler were prepared by solution casting method. In these composite films, using TSP as the reducing agent, silver nanoparticles (AgNPs) were in situ generated using 1 to 5 mM aq. $AgNO_3$ source solutions. The hybrid nanocomposite films were characterized by FTIR spectroscopy, X-ray diffraction, scanning electron microscopy (SEM), polarized optical microscopy (POM), tensile testing, thermogravimetric analysis, and antibacterial studies. From the SEM analysis, it was evident that the particle size of the AgNPs varied between 44 and 86 nm when 1 to 4 mM source solutions were used. But on the other hand, the particle size increased to 406 nm when 5 mM source solution was used indicating agglomeration of the AgNPs. The reinforcement of TSP enhanced the crystallinity of the poly(propylene carbonate) (PPC) matrix. The hybrid nanocomposite films exhibited enhanced tensile and thermal properties when compared with the PPC matrix. Further, the hybrid nanocomposites exhibited excellent antibacterial properties against *Escherichia coli* (*E. coli*), *Pseudomonas aeruginosa* (*P. aeruginosa*), *Bacillus licheniformis* (*B. licheniformis*) and *Staphylococcus aureus* (*S. aureus*) bacteria. These hybrid nanocomposites with excellent tensile and antibacterial properties can be potentially used for food packaging applications.

Keywords Poly(propylene)carbonate · Tamarind seed polysaccharide · Silver nanoparticles · In situ generation · Tensile strength · Antibacterial activity

✉ Nallamuthu N.
nnallamuthu@gmail.com

✉ Rajini N.
rajiniklu@gmail.com

Indira Devi M.P.
indirarajini20@gmail.com

Senthil Muthu Kumar T.
tsmkumar@klu.ac.in

Suchart Siengchin
suchart.s.pe@tggs-bangkok.org

Varada Rajulu A.
arajulu@rediffmail.com

Hariram N.
n.hariram@klu.ac.in

[1] Department of Physics, Kalasalingam Academy of Research and Education, Krishnankoil, Tamil Nadu 626126, India

[2] Department of Mechanical Engineering, Kalasalingam Academy of Research and Education, Krishnankoil, Tamil Nadu 626126, India

[3] Department of Mechanical and Process Engineering, The Sirindhorn International Thai German Graduate School of Engineering (TGGS), King Mongkut's University of Technology North Bangkok, Bangkok 10800, Thailand

[4] Centre for Composite Materials, International Research Centre, Kalasalingam Academy of Research and Education, Krishnankoil, Tamil Nadu 626126, India

[5] Department of Biotechnology, Kalasalingam Academy of Research and Education, Krishnankoil, Tamil Nadu 626126, India

Introduction

Today, the impact of the plastic food packaging materials on the environment includes the utilization of resources for packaging production, environmental pollution caused by the process and disposal [1, 2]. On the other hand, there is a huge demand for microwave food, frozen food, and snacks from the consumers. The packaging materials must therefore offer a balanced advantage on both food protection and environmental protection [3]. Accordingly, many works have been reported using different biodegradable polymers such as cellulose [4], starch [5, 6] soy proteins [7], polylactides [8], polyhydroxyalkanoates [9], poly(vinyl alcohol) [10], with reinforcing fillers for packaging applications. Similarly, poly(propylene carbonate) (PPC) is also a biodegradable polymer which is synthesized by reaction of CO_2 and propylene oxide in the presence of catalyst [11]. In PPC matrix, several biofillers have been reinforced for improving its properties. Some of them are spent tea leaf powder [12], spent coffee bean powder [13], egg shell powder [14], wood flour [15], cellulose nanocrystals [16], tamarind nut powder [17] etc.

Polymer composites can potentially be used as food packaging materials and can be categorized into three types based on the purpose of usage such as improved packaging, active packaging, and intelligent packaging [18]. Using fillers with nano-size can be a promising option to improve the functional properties [6] of the composites. In recent years, nano metals and metal oxides of silver, zinc, magnesium etc. [19] were used to improve the properties such as flexibility, gas barrier, and antimicrobial or antioxidant properties [20] of polymer composites. The interaction and the compatability between the filler and the matrix is an important factor to achieve the reinforcing effect of nanocomposites. Mainly the properties of the nanocomposites depend on the size of the filler, its dispersion, and the interfacial bonding [21]. Further, the incorporation of nanofillers with antimicrobial or antioxidant activities can result in an inhibiting effect on the microbial growth which can protect the food from spoiling. Silver nanoparticles are most widely used in laundry detergents, disinfectant sprays, and kitchen utensils to inhibit the growth of microorganisms. They are also effective against Gram-positive and Gram-negative bacteria and have a significant antimicrobial performance against multidrug-resistant microorganisms [22, 23]. When silver nanoparticles are incorporated and immobilized in a polymer film by in situ generation, the particles disperse evenly [24] and retain their nano-size in the films. Such films help in extending the shelf life of the food materials [25]. But there can be potential hazard to the consumer health if there is a migration of the nanoparticles into the food stuff. The antibacterial effect in food packaging applications can be performed without the migration of the silver nanoparticles, with the polymer acting as carriers of silver nanoparticles [26]. To the best of our knowledge, there are no reports on using PPC-based hybrid nanocomposites targeting the food packaging application. Hence, in the present work, it was proposed to in situ generate the silver nanoparticles (AgNPs) in the biodegradable polymer composite films with poly (propylene) carbonate and tamarind seed polysaccharide. The hypothesis is that the addition of silver nanoparticles increases the antibacterial properties, and addition of tamarind seed polysaccharide increases the thermal and mechanical properties, while also reducing the final cost of the material.

In this work, hybrid nanocomposite films were fabricated with two different fillers into PPC matrix, namely, tamarind seed polysaccharide (TSP) and the generated AgNPs using solution casting and in situ generation methods. The effect of in situ generated AgNPs on the functional properties of PPC/TSP matrix system was studied. It was proved that the resulting hybrid nanocomposites with better functional properties could be a possible alternate in the food packaging applications.

Materials and methods

Materials

Poly(propylene) carbonate (PPC) was procured from Tianguan Enterprise Group Company (Henan, China) in the form of pellets. The tamarind seed polysaccharide and dimethyl formamide (DMF) were purchased from the local market, India. Silver nitrate ($AgNO_3$) was purchased from Sigma-Aldrich (Mumbai, India). Standard and clinically isolated microorganism strains of Gram-negative *Escherichia coli* (*E. coli*) and *Pseudomonas aeruginosa* (*P. aeruginosa*) and Gram-positive *Staphylococcus aureus* (*S. aureus*) and *Bacillus licheniformis* (*B. licheniformis*) were procured from MTCC, IMTECH, Chandigarh, India, and were used for antimicrobial assays.

Preparation of poly(propylene) carbonate/tamarind seed polysaccharide/silver nanoparticle hybrid nanocomposites

The TSP was dried in a hot air oven at 100 °C for 1 h to remove the moisture content. With the aid of a sieve, the powder with particle size less than 20 μm was separated and mixed with the PPC solution using a mechanical stirrer. Prior to this, the PPC solution was prepared for the required wt% using the same procedure reported earlier [12, 14]. The mixture of PPC/TSP solution was spread over the glass plate to obtain the uniform thickness as per the spacer dimension. Then, the PPC/TSP composite films were formed using simple casting technique. The composite films were then dipped in 1 to 5 mM aq.$AgNO_3$ source solutions separately to get in

situ generated AgNPs in the films to form hybrid nanocomposites. The films with change in color were washed thoroughly with distilled water and then dried. The color remained unchanged despite repeated washings with distilled water indicating the permanent generation of AgNPs in the hybrid nanocomposite films. Then, films were stored in desiccators prior to further testing.

Microscopy

A scanning electron microscope (SEM) (Zeiss O 18) and a polarized optical microscope with a digital image analyzer (Olympus SZX12) were used to investigate the distribution and particle size of the TSP fillers and the AgNPs in the nanocomposite films.

Fourier transform infrared spectroscopy

An IR spectrometer (Bruker Vector 22) was used to record the Fourier transform infrared spectroscopy (FTIR) spectra of the PPC matrix, the filler, and the PPC/TSP/AgNPs hybrid nanocomposites in reflection mode. All the spectra were recorded in the 4000–500 cm^{-1} region with 32 scans in each case, at a resolution of 4 cm^{-1}.

X-ray diffraction

An X-ray diffractometer (Rigaku Corporation, Japan) was used to record X-ray diffractograms of the PPC/TSP/AgNPs hybrid nanocomposites in 10-80° range at a scan rate of 4°/min.

Thermogravimetric analysis

The primary and derivative thermograms of the PPC/TSP composite matrix and the PPC/TSP/AgNPs hybrid nanocomposite films were recorded using a thermogravimetric analyzer (Mettler Toledo) in the temperature range of 25–600 °C in nitrogen atmosphere at a heating rate of 10 °C/min.

Tensile testing

The tensile properties of PPC/TSP composite matrix and PPC/TSP/AgNPs hybrid nanocomposite films were determined as per the ASTM D882 specifications. Film strips were cut into 100 mm × 10 mm sections and then characterized using INSRON 3369 Universal tensile machine equipped with 5 KN load cell with an initial grip separation and crosshead speeds of 50 mm and 5 mm/min, respectively. Tensile strength, modulus, and elongation at break were calculated. Five identical specimens were used in each case, and the average values are reported.

Antibacterial activity

The antibacterial test conducted for the hybrid nanocomposite films was carried against four bacteria using two Gram-negative namely *Escherichia coli* (*E. coli*) and *Pseudomonas aeruginosa* (*P. aeruginosa*) and two Gram-positive *Staphylococcus aureus* (*S. aureus*) and *Bacillus licheniformis* (*B. licheniformis*) by disc method as described elsewhere [27]. The inhibition zones indicating the inhibition of bacteria were photographed, and the zone diameter in each case was measured. All test organisms were inoculated in LB broth (pH 7.0.) for 8 h. The concentration of the suspensions was adjusted to 0.5 (optical density) by using a spectrophotometer. Isolates were seeded on LB agar plates by using sterilized sterile plastic inoculation loop and L rod. One hundred microliters of 10–6 cells was spread over the LB agar plate. Plates were incubated at 37 °C for 48 h. Triplicate plates were maintained for each organism.

Results and discussion

Appearance of the matrix and the PPC/TSP/AgNPs hybrid nanocomposite films

The digital images of the matrix and the PPC/TSP/AgNPs hybrid nanocomposite films are shown in Fig. 1. From Fig. 1, it is evident that both the matrix and the PPC/

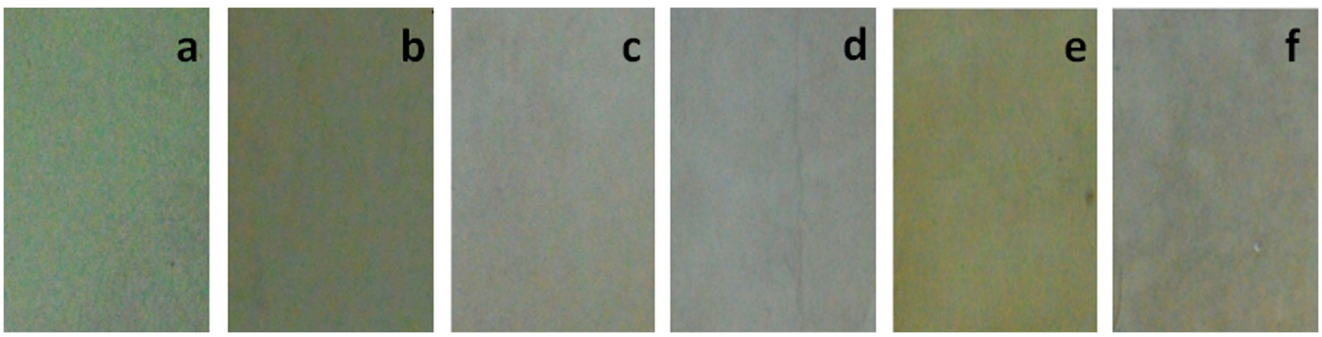

Fig. 1 Digital images of PPC/TSP matrix (**a**) and PPC/TSP/AgNPs hybrid nano composite films made using 1 mM (**b**), 2 m (**c**), 3 mM (**d**), 4 mM (**e**), and 5 mM (**f**) aq.$AgNO_3$ source solutions

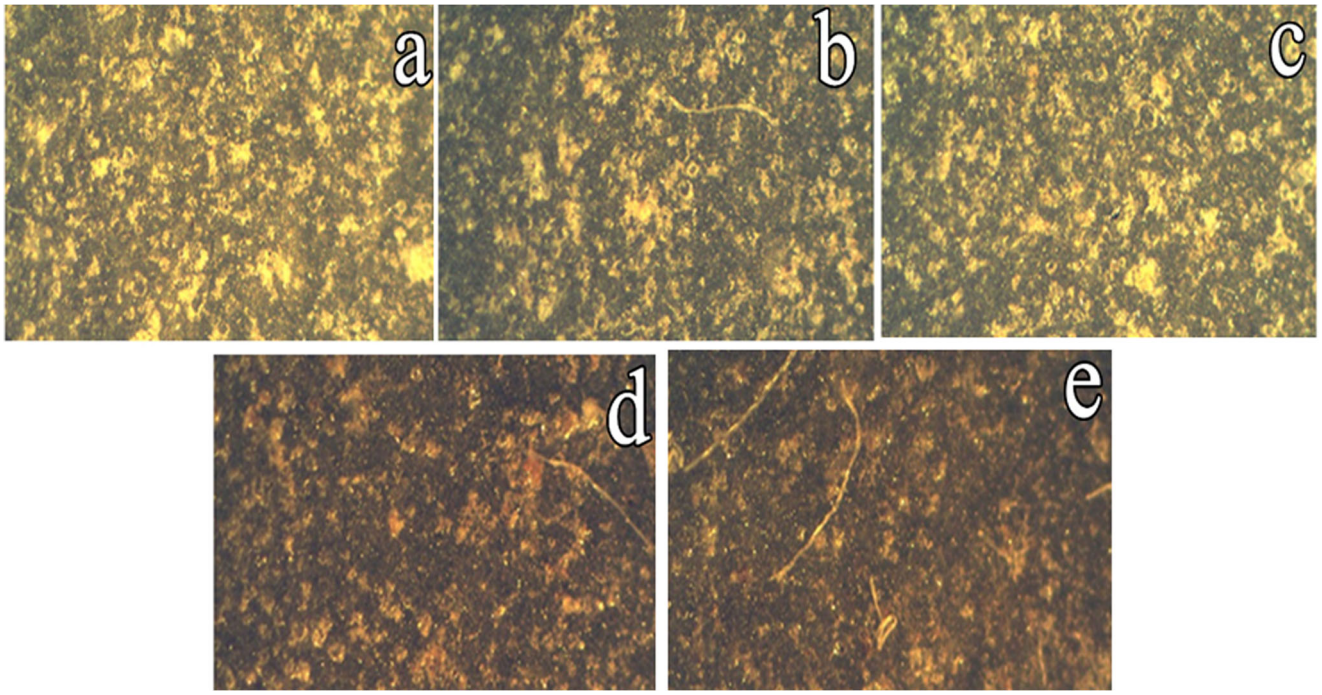

Fig. 2 Optical images of PPC/TSP/AgNPs hybrid nanocomposites made using 1 mM (**a**), 2 m (**b**), 3 mM (**c**), 4 mM (**d**), and 5 mM (**e**) aq.$AgNO_3$ source solutions

TSP/AgNPs hybrid nanocomposite films were uniform. As the TSPs have proteins, carbohydrates, crude fibers etc., in order to probe the presence of the crude fibers, the polarized optical micrographs were recorded and are presented in Fig. 2. From Fig. 2, we can observe, in addition to the carbohydrate particles, the nanocomposite films had some fibers [28] which could not be observed in the digital images (Fig. 1). The presence of the fibers in the fillers of the nanocomposites is expected to improve their tensile properties. Further, from the digital images of the composite films, it can be understood that, upon increasing the filler concentration, the color of the films darkened, but they

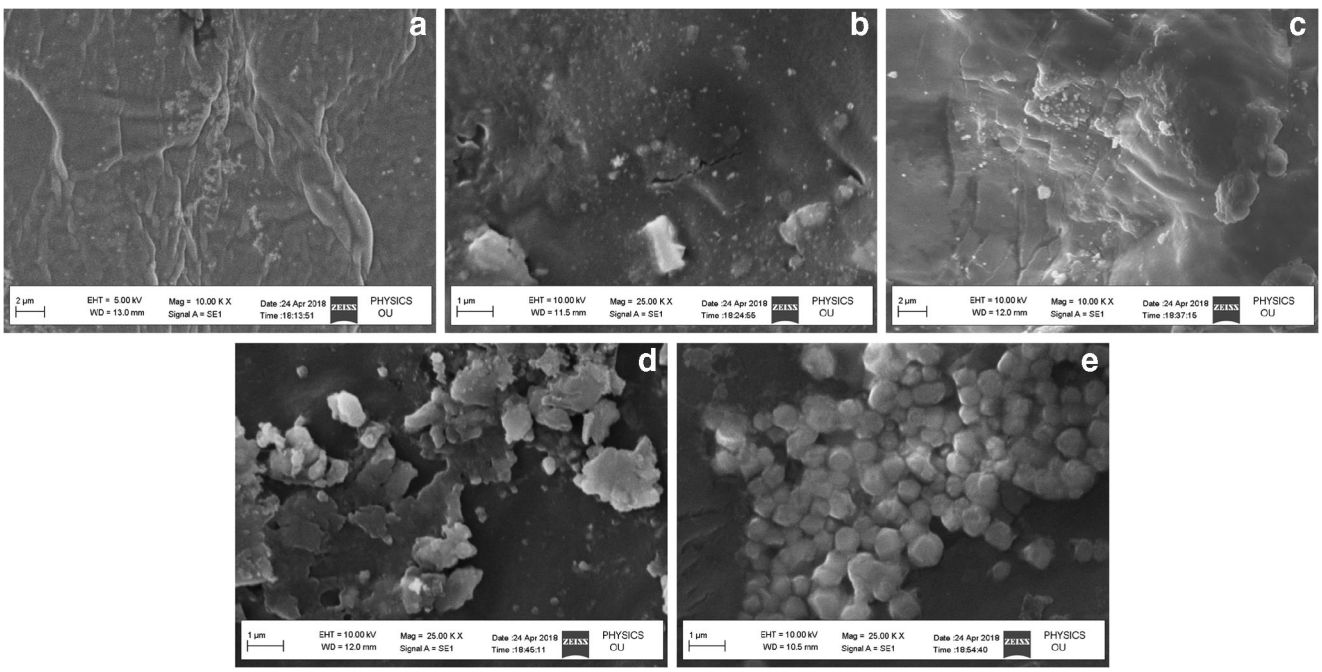

Fig. 3 SEM images of PPC/TSP/AgNPs hybrid nanocomposite films with in situ generated AgNPs on the surface of the TSPs made using 1 mM (**a**), 2 mM (**b**), 3 mM (**c**), 4 mM (**d**), and 5 mM (**e**) aq.$AgNO_3$ source solutions

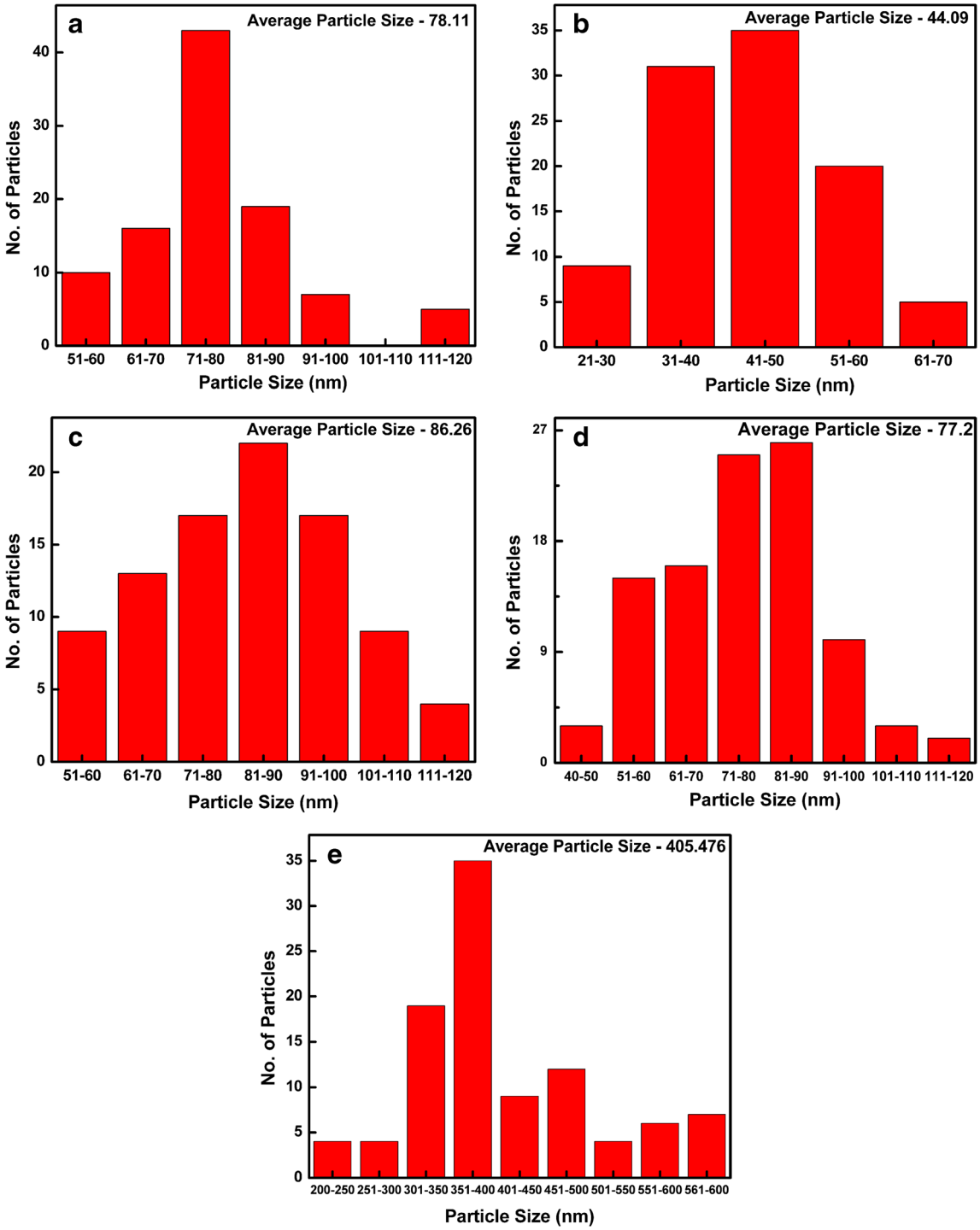

Fig. 4 Histograms of the particle size distribution of in situ generated AgNPs in the PPC/TSP/AgNPs hybrid nanocomposite films made using 1 mM (**a**), 2 mM (**b**), 3 mM (**c**), 4 mM (**d**), and 5 mM (**e**) aq.$AgNO_3$ source solutions

have sufficiently enough transparency. Hence, they can also be utilized for wrapping applications.

SEM analysis

The SEM images of the PPC/TSP/AgNPs hybrid nanocomposite films are presented in Fig. 3. From Fig. 3, it can be seen that the nanocomposite films had spherical AgNPs on the surface of the TSP filler. It can also be observed that with the increase in the concentration of the source solution, the resulting AgNPs were found to agglomerate at some places. The particle size in each case was measured using SmartTiff program, and the histograms indicating the particle size distribution are presented in Fig. 4.

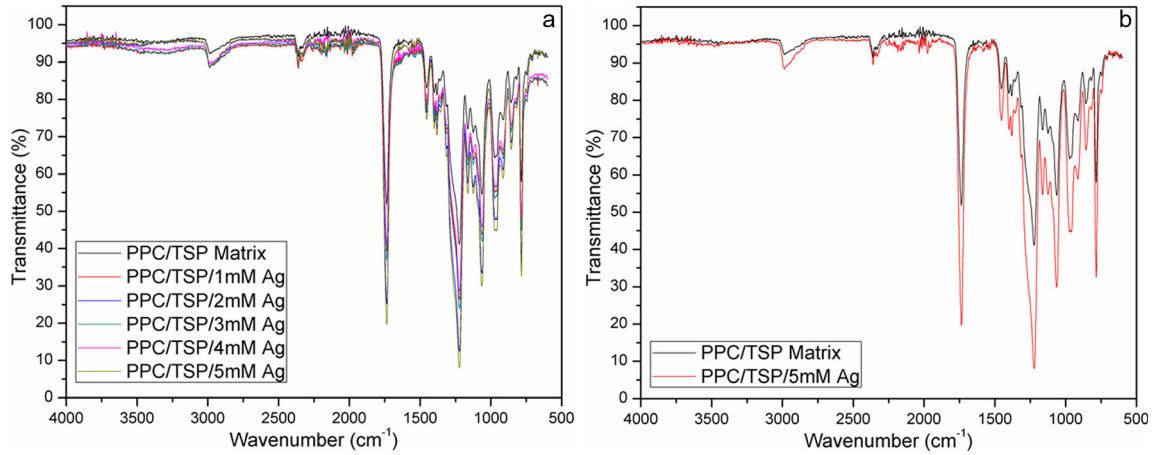

Fig. 5 FTIR spectra of PPC/TSP (Matrix) and PPC/TSP/AgNPs hybrid nanocomposite films made using 1 to 5 mM aq.$AgNO_3$ source solutions (**a**) and PPC/TSP and PPC/TSP/AgNPs composite film made using 5 mM aq.$AgNO_3$ source solution (**b**)

From Fig. 4, it is evident that the average particle size when the 1 to 4 mM source solutions were used varied between 44 and 86 nm. However, when 5 mM source solution was used, the average size of the AgNPs was found to be around 406 nm indicating agglomeration of the particles. It is understandable as for the highest concentrated source solution, many number of AgNPs were generated leading to their agglomeration. It is worthy to note here that the agglomeration of the AgNPs did not affect the tensile strength and modulus of the hybrid nanocomposites. It can be seen that the tensile strength and modulus had an increasing trend even at the highest source solution concentration.

Fourier transform infrared spectroscopy analysis

The FTIR spectra of the matrix and the composite films were recorded and presented in Fig. 5a. From Fig. 5a, it is evident that the spectra of both the matrix and the hybrid nanocomposite films were similar. For clarity, the spectra of the matrix and the PPC/TSP/AgNPs composite film made using 5 mM aq.$AgNO_3$ source solution are presented separately in Fig. 5b. From Fig. 5b, it is evident that the matrix and the hybrid nanocomposite film had similar functional groups. The broad and shallow absorption band at 3500 cm^{-1} corresponds to the stretching vibrations of the OH groups of TSP. The bands at 2995 and 1730 cm^{-1} correspond to the C–H and C=O stretching vibrations. Further, the peaks at 1460 and 1237 cm^{-1} were attributed to the –C–H bending and –CO vibrations of carbonate. The C–C of methyl group resulted a peak at 941 cm^{-1} while the deformation of the methylene group at 780 cm^{-1}. The sharp band at 1066 cm^{-1} was ascribed to the C–O–C vibrations [17]. Hence, the in situ generated AgNPs in the TSP filler did not alter the structure of the hybrid nanocomposite films.

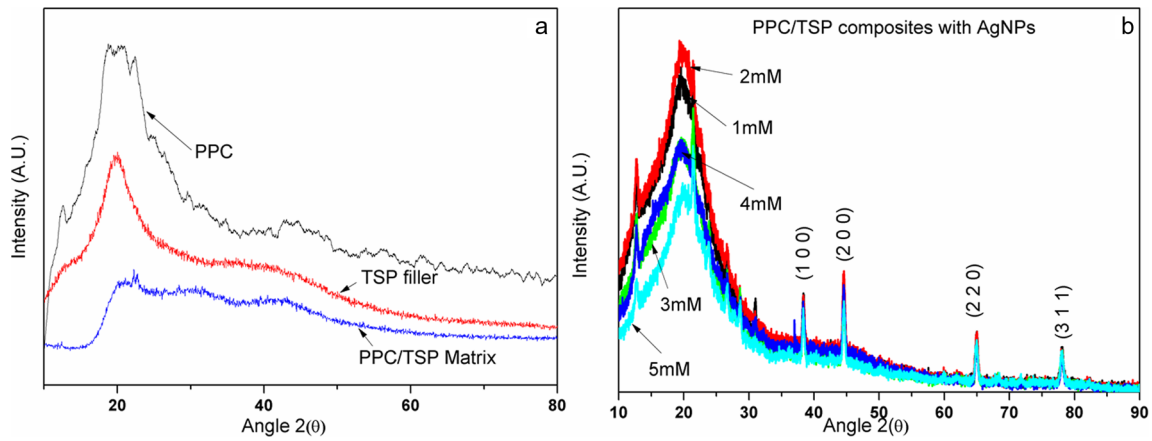

Fig. 6 XRD pattern of **a** pure PPC, TSP filler and matrix (PPC/TSP composite) and PPC/TSP/AgNPs hybrid nanocomposite films made using 1 mM (**a**), 2 mM (**b**), 3 mM (**c**), 4 mM (**d**), and 5 mM (**e**) aq.$AgNO_3$ source solutions

Table 1 The FWHM (B_{size}) and crystallite size (Dp) of PPC/TSP/AgNPs composites with in situ generated AgNPs using 1 mM, 2 mM, 3 mM, 4 mM, and 5 mM aq.$AgNO_3$ source solutions

Peak position 2θ (°)	1 mM AgNPs		2 mM AgNPs		3 mM AgNPs		4 mM AgNPs		5 mM AgNPs	
	FWHM B_{size} (°)	Dp (nm)	FWHM B_{size} (°)	Dp (nm)	FWHM B_{size} (°)	Dp (nm)	FWHM B_{size} (°)	Dp (nm)	FWHM B_{size} (°)	Dp (nm)
38.37	0.62742	14.01	0.87441	10.05	0.56338	15.61	0.7402	11.88	0.5723	15.36
44.57	0.52076	17.23	0.54729	16.4	0.56342	15.93	0.6329	14.18	0.5629	15.94
65.01	0.54107	18.2	0.5444	18.09	0.52497	18.76	0.4983	19.76	0.5597	17.59
78.07	0.59124	18.08	0.59549	17.95	0.49158	21.75	0.5446	19.63	0.6081	17.58
Dp Average (nm)		16.88		15.62		18.01		16.36		16.62

X-ray diffraction analysis

The PPC, TSP filler, and PPC/TSP composites and PPC/TSP/AgNPs hybrid nanocomposites were characterized using X-ray diffraction (XRD) to comprehend the structural behavior. Figure 6a shows the XRD spectra of PPC, TSP filler, and PPC/TSP composites. The appearance of a broad peak indicates the amorphous nature of PPC. Similar observation was also reported earlier [29, 30]. Further, the presence of sharp intensified peak at 2θ = 20° was attributed to the crystalline nature of TSP filler with cellulose-II structure. From Fig. 6a, it is clearly evident that the addition of TSP filler in the matrix influenced the intensity of the peak in the case of PPC/TSP composites [17]. Figure 6b shows the XRD spectra for PPC/TSP/AgNPs hybrid nanocomposites with in situ generated AgNPs made using 1 to 5 mM aq.$AgNO_3$ source solutions. Strong peaks appeared at 2θ = 38.37°, 44.57°, 65.01°, and 78.07° corresponding to the reflections from (111), (200), (220), and (311) planes of AgNPs in the hybrid nanocomposite films. Such observations were also made for AgNPs in similar systems [31–33]. Besides, the peak at 32.28° might be due to the organic compounds in the TSP filler [34]. A similar result was reported earlier, where they identified the crystalline peaks at 32.28° [34, 35].

Further, the crystallite size of the AgNPs was determined using Debye–Scherrer's equation as reported earlier [36]:

$$\text{Crystallite size } D_A = K\,\lambda/(B\cos\theta)$$

where D_A—average crystallite size (nm); **K**—Scherrer constant. **K** varies from 0.68 to 2.08. **K** = 0.94 for spherical crystallites with cubic symmetry; **λ**—X-ray wavelength, Cu Kα radiation (1.54178 Å); **B**—FWHM (Full width at half maximum) of XRD peak; **θ**—XRD one half of 2θ peak position. The average crystallite size values for PPC/TSP composites with in situ generated AgNPs using 1 to 5 mM aq.$AgNO_3$ source solutions are presented in Table 1. The calculated crystallite sizes are in good agreement with the reported values published by earlier workers for AgNPs [31–33]. The calculated average size of the particle is 16.8 nm, 15.6 nm, 18.0 nm, 16.3 nm, and 16.2 nm for the PPC/TSP/AgNPs hybrid nanocomposites with in situ generated AgNPs using 1 mM, 2 mM, 3 mM, 4 mM, and 5 mM aq.$AgNO_3$ source solutions respectively.

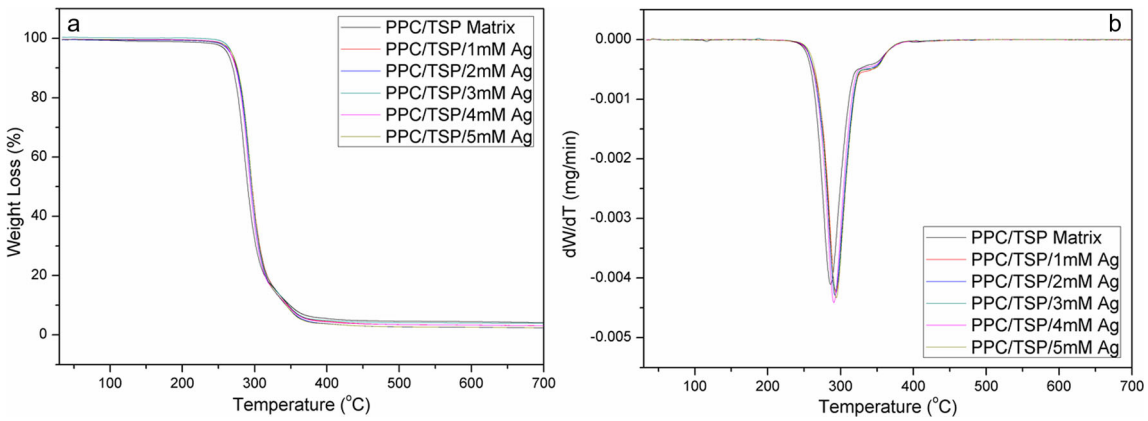

Fig. 7 Primary thermograms (**a**) and derivative thermograms (**b**) of matrix and PPC/TSP/AgNPs hybrid nanocomposite films made using 1 to 5 mM aq.$AgNO_3$ source solutions

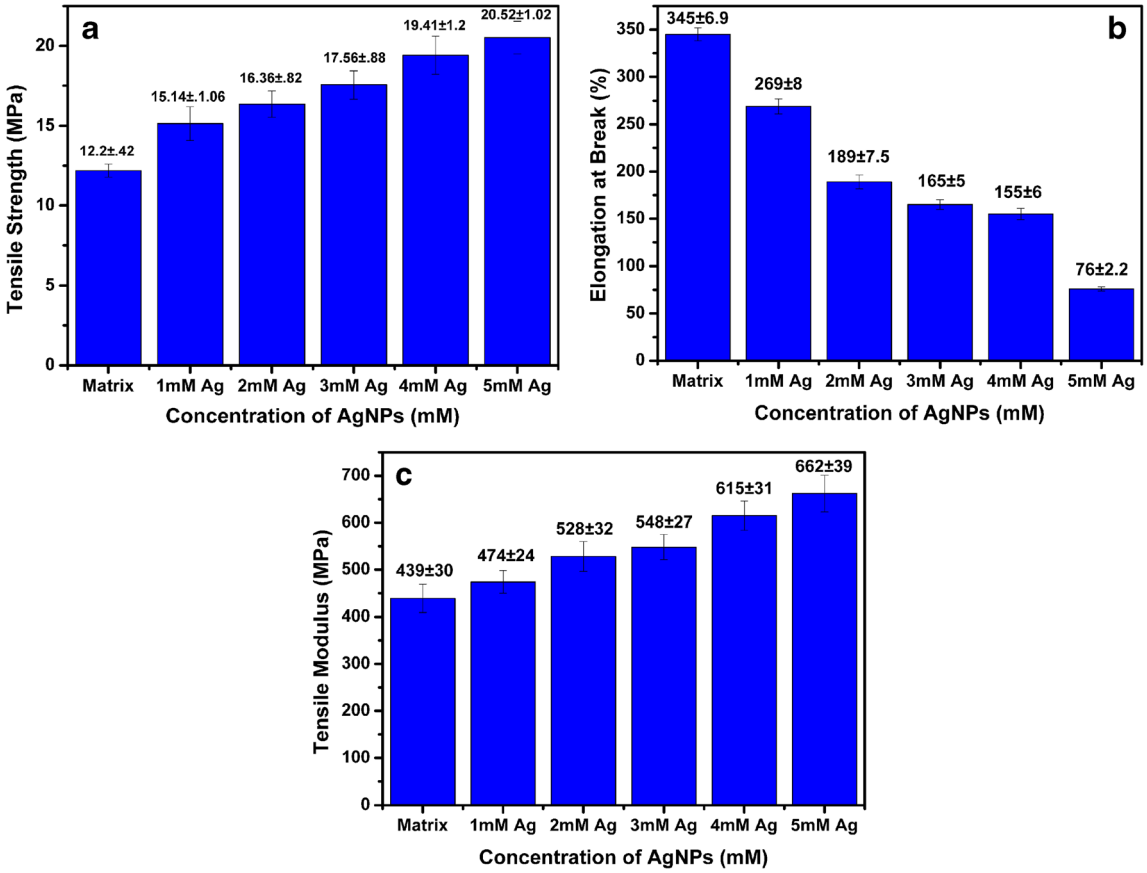

Fig. 8 Tensile strength (**a**), tensile modulus (**b**), and %elongation at break (**c**) of the matrix and the PPC/TSP/AgNPs hybrid nanocomposite films made using 1 to 5 mM aq.$AgNO_3$ source solutions

Thermogravimetric analysis

In order to probe the thermal stability of the PPC/TSP/AgNPs hybrid nanocomposites, the thermogravimetric analysis was performed and the results are presented in Fig. 7. It can be noticed that there is no inflection peak found in the region of 30–100 °C, indicating the hydrophobic nature of PPC. From Fig. 7, it is evident that the thermal stability of the composites increased with increase in filler content. However, till a temperature of 350 °C, the thermal stability of the composites was lower than the matrix but after that, a reverse trend was observed. This could be attributed to the polyphenols present in the TSP filler [17] and also the nanoparticles could have influenced such an effect. Further, the thermal stability of the composites could be attributed to the presence of crystalline polysaccharides in the TSP which include cellulose and carbohydrates.

Tensile properties

In order to probe the effect of in situ generated AgNPs on the tensile properties of the PPC/TSP/AgNPs hybrid nanocomposite films, the tensile test was carried out. The histograms representing the tensile strength, tensile modulus, and the % elongation at break of the matrix and the PPC/TSP/AgNPs hybrid nanocomposite films are presented in Fig. 8. The tensile properties of the matrix (PPC/TSP composite) used in the present work were compared with those of same grade PPC used in the earlier work of one of our groups [12]. The tensile strength, modulus, and elongation at break of PPC were reported to be 10.5 MPa, 417 MPa, and 821%, respectively. From Fig. 8, it can be observed that the tensile strength and modulus of PPC/TSP composite used in the present work increased by 16 and 5% while the elongation at break decreased by 138% over the PPC. This may be due to the presence of microfibers and polyphenols in the TSP. Further, from Fig. 8, it is evident that the tensile strength and the modulus of the hybrid nanocomposite films were higher than those of the matrix and increased with increasing concentrations of the source solutions. However, the % elongation at break exhibited a reverse trend. The possible reasons for such a trend could be the uniform dispersion of the TSP fillers with in situ generated rigid AgNPs in the PPC/TSP/AgNPs hybrid nanocomposites. Further, the effective stress transfer among

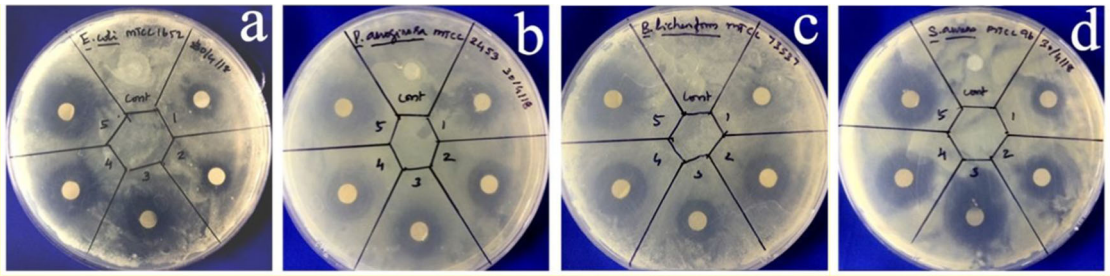

[After 24 hours]

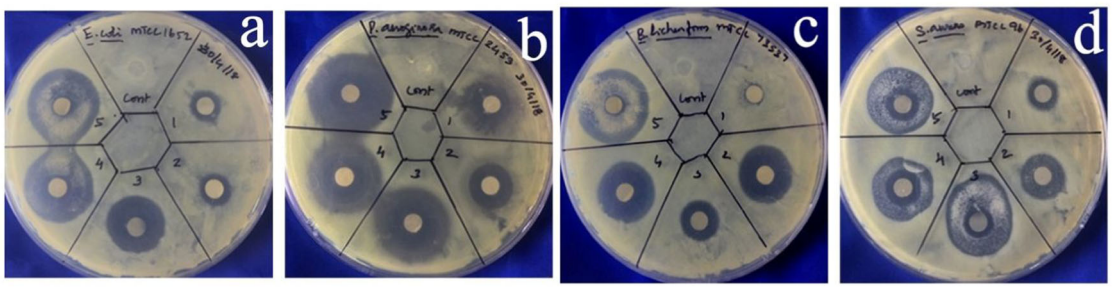

[After 36 hours]

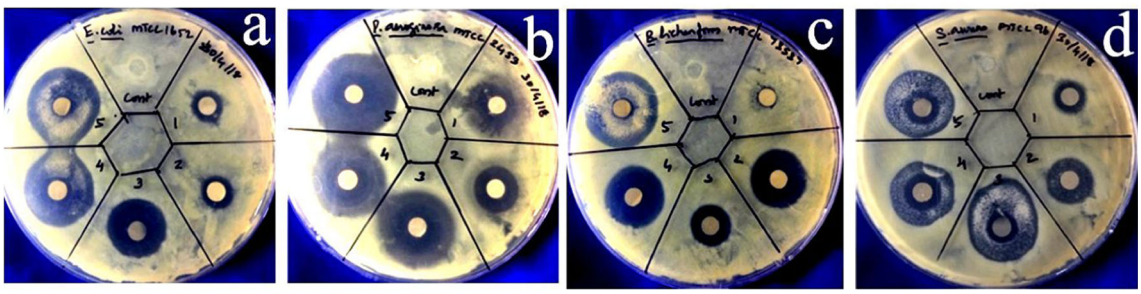

[After 48 hours]

Fig. 9 Antibacterial inhibition zones of PPC matrix and PPC/TSP/AgNPs hybrid nanocomposite films made using 1 mM (1); 2 mM (2); 3 mM (3); 4 mM (4), and 5 mM (5) aq.$AgNO_3$ source solutions against *Escherichia coli* MTCC 1652 (**a**), *Pseudomonas aeruginosa MTCC 2453* (**b**), *Bacillus licheniformis MTCC 73537* (**c**), and *Staphylococcus aureus MTCC 96* bacteria [after 24 h, 36 h, and 48 h]

the components may be another reason for the improvement in the tensile properties of the hybrid nanocomposite films under study [10, 37]. Similar observation was also made in the case of PPC/TNP composites [17] and cellulose/TNP composites [38].

Antibacterial activity

It is an established fact that the AgNPs exhibit good antibacterial activity. In order to probe the antibacterial activity of the PPC/TSP/AgNPs hybrid nanocomposite films, the antibacterial test by disc method was carried out against both Gram-negative and Gram-positive bacteria. The zones of clearance indicating the inhibition of bacteria were photographed after 24 h, 36 h, and 48 h, and the respective images photographed are presented in Fig. 9. Results were analyzed on the basis of diameter of inhibition zones of nanocomposite films with varying concentration of AgNPs under different bacterial medium. From Fig. 9, it is evident that though the matrix did not exhibit any antibacterial activity, the nanocomposite films showed good antibacterial activity against both Gram-negative (*Escherichia coli* and *Pseudomonas aeruginosa*) and Gram-positive (*Bacillus licheniformis* and *Staphylococcus aureus*) bacteria after 24 h, 36 h, and 48 h of the test. Further, in all the cases, the

diameters of the clear zones increased with increasing concentration of the source solutions.

From the result, a slight increase in clear zone diameter was observed for the particular bacteria in each case of Gram-negative (*P. aeruginosa*) and Gram-positive (*S. aureus*) at 36 and 48 h of inhibition. It could happen because of highly sensitive nature and chemical structure of *P. aeruginosa* than that of *E. coli* bacteria though both belong to Gram negatives. A similar observation was also found for *S. aureus* in Gram-positive case because of a compound nature. However, it was observed that the clear zone formation was found to vary due to various factors such as type of bacterial medium, concentration, cell wall mechanism etc. Some of the previous reports discussed about the restriction of antibiotic behavior of bacteria through various mechanisms have been considered to support the aforesaid statements. Accordingly, some microorganisms are capable of changing the antibiotic's chemical structure. This mechanism is applicable in bacteria which produce β-lactamases, and these enzymes cleave the β-lactam ring of the penicillin, or other β-lactams, which leaves the antibiotic obsolete [39]. Secondly, some bacteria have an increased number of efflux pumps in their cellular membrane. These efflux pumps can rapidly expel the antibiotic that enters the cell, keeping the internal antibiotic concentration to a minimum [40]. Lastly, bacteria also have the ability to modify chemically or genetically the target site of the antibiotic, and hence, once the target is modified, the antibiotic cannot bind and resistance is acquired [41]. Further, increasing concentration of $AgNO_3$ could lead to the increasing surface area of nanoparticles which in turn can have interactions with larger microorganisms and thus alter the microbial metabolism [42]. It is well known that AgNPs are toxic to microorganisms, and hence, the AgNPs embedded TSP filler in the nanocomposite films are expected to lysis the cell wall of the bacteria and restrict the further growth of bacteria [42, 43]. After the formation of antimicrobial activity in the AgNP compound, the retention of clear zone was not found to occur even after 48 h of inhibition which could confirm the effectiveness of AgNPs present in the medium. It ensures the stability of the AgNP compound in the medium which can happen due to the existence of Ag nanoparticle after the oxidation process.

Conclusions

The AgNPs were in situ generated in the PPC/TSP composite films to form hybrid nanocomposites. The average particle size of the AgNPs was found to be 44 to 86 nm when 1 to 4 mM source solutions were used. On the other hand, when 5 mM source solution was used, there was an increase in the particle size to 406 nm which evidence the formation of particle agglomeration. The infusion of TSP in the PPC matrix increased the crystallinity. The FTIR spectra were almost similar for both the matrix and composites indicating no changes in the structure of the composites. The XRD diffractograms proved that the crystallinity of the composites increased with the addition of fillers. The hybrid nano composite films exhibited better thermal stability compared to the matrix. This may be attributed to the rigid polyphenols and polysaccharides present in the TSP filler and the presence of AgNPs. The tensile strength and modulus of the composites increased with increase in the filler content, while a reverse trend was observed in case of % elongation at break. This behavior of the nanocomposite films may be due to the in situ generation of rigid AgNPs in them which increased the tensile stress and modulus while decreasing the % elongation at break. Further, the films exhibited excellent antibacterial activity against both Gram-positive and Gram-negative bacteria. These hybrid nanocomposite films with excellent tensile and antibacterial properties can be potentially used in active food packaging applications.

Acknowledgements The authors are thankful to the authorities of Kalasalingam Academy of Research and Education, Tamil Nadu, India, for supporting this research by providing fabrication facilities.

Funding information Department of Science and Technology, India, provided funding through Young Scientist Start up Scheme YSS/2015/001353 project.

References

1. Lewis H (2008) Eco-design of food packaging materials. In: Chiellini E (ed) Environmentally compatible food packaging. Woodhead Publishing Limited, Cambridge, pp 238–262
2. Guo G, Xiang A, Tian H (2018) Thermal and mechanical properties of eco-friendly poly(vinyl alcohol) films with surface treated bagasse fibers. J Polym Environ 26(9):3949–3956
3. Lau OW, Wong SK (2000) Contamination in food from packaging material. J Chromatogr A 882:255–270
4. Duan J, Obi Reddy K, Ashok B, Cai J, Zhang L, Rajulu AV (2016) Effects of spent tea leaf powder on the properties and functions of cellulose green composite films. J Environ Chem Eng 4:440–448
5. Dai L, Qiu C, Xiong L, Sun Q (2015) Characterization of corn starch-based films reinforced with taro starch nanoparticles. Food Chem 174:82–88
6. Tian H, Yan Y, Rajulu AV, Xiang A, Luo X (2017) Fabrication and properties of polyvinyl alcohol/starch blend films: effect of composition and humidity. Int J Biol Macromol 96:518–523
7. Tian H, Xu G (2011) Processing and characterization of glycerol-plasticized soy protein plastics reinforced with citric acid-modified starch nanoparticles. J Polym Environ 19(3):582–588
8. Ashok B, Naresh S, Obi Reddy K, Madhukar K, Cai J, Zhang L, Rajulu AV (2014) Tensile and thermal properties of poly(lactic acid)/eggshell powder composite films. Int J Polym Anal Charact 19(3):245–255

9. Xiang HX, Chen SH, Cheng YH, Zhou Z, Zhu MF (2013) Structural characteristics and enhanced mechanical and thermal properties of full biodegradable tea polyphenol/poly(3-hydroxybutyrate-co-3-hydroxyvalerate) composite films. Express Polym Lett 7(9):778–786
10. Tian H, Wang K, Liu D, Yan Y, Xiang A, Rajulu AV (2017) Enhanced mechanical and thermal properties of poly (vinyl alcohol)/corn starch blends by nanoclay intercalation. Int J Biol Macromol 101:314–320
11. Chisholm MH, Zhou Z (2004) Concerning the mechanism of the ring opening of propylene oxide in the copolymerization of propylene oxide and carbon dioxide to give poly (propylene carbonate). J Am Chem Soc 126(35):11030–11039
12. Xia G, Obi Reddy K, Uma Maheswari C, Jayaramudu J, Zhang J, Zhang J, Rajulu AV (2015) Preparation and properties of biodegradable spent tea leaf powder/poly(propylene carbonate) composite films. Int J Polym Anal Charact 20(4):377–387
13. Senthil Muthu Kumar T, Rajini N, Tian H, Rajulu AV, Ayrilmis N, Siengchin S (2018) Improved mechanical and thermal properties of spent coffee bean particulate reinforced poly(propylene carbonate) composites. Part Sci Technol. https://doi.org/10.1080/02726351.2017.1420116
14. Feng Y, Ashok B, Madhukar K, Zhang J, Zhang J, Obi Reddy K, Rajulu AV (2014) Preparation and characterization of polypropylene carbonate bio-filler (eggshell powder) composite films. Int J Polym Anal Charact 19(7):637–647
15. Nornberg B, Borchardt E, Luinstra GA, Fromm J (2014) Wood plastic composites from poly(propylene carbonate) and poplar wood flour—mechanical, thermal and morphological properties. Eur Polym J 51:167–176
16. Jiang G, Zhang M, Feng J, Zhang S, Wang X (2017) High oxygen barrier property of poly(propylene carbonate)/polyethylene glycol nanocomposites with low loading of cellulose nanocrytals. ACS Sustain Chem Eng 5:11246–11254
17. Senthil Muthu Kumar T, Rajini N, Tian H, Rajulu AV, Jappes JTW, Siengchin S (2017) Development and analysis of biodegradable poly(propylene carbonate)/tamarind nut powder composite films. Int J Polym Anal Charact 22(5):415–423
18. Chaudhry Q, Scotter M, Blackburn J, Ross B, Boxall A, Castle L, Aitken R, Watkins R (2008) Applications and implications of nanotechnologies for the food sector. Food Addit Contam A 25(3):241–258
19. Jones CM, Hoek EMV (2010) A review of the antibacterial effects of silver nanomaterials and potential implications for human health and the environment. J Nanopart Res 12(5):1531–1551
20. Echegoyen Y, Nerin C (2013) Nanoparticle release from nanosilver antimicrobial food containers. Food Chem Toxicol 62:16–22
21. Liu D, Yuan L, Xu H, Tian H, Xiang A (2018) PVA grafted POSS hybrid for high performance polyvinyl alcohol films with enhanced thermal, hydrophobic and mechanical properties. Polym Compos. https://doi.org/10.1002/pc.25084
22. Birla SS, Tiwari VV, Gade AK, Ingle AP, Yadav AP, Rai MK (2009) Fabrication of silver nanoparticles by phoma glomerata and its combined effect against *Escherichia coli, Pseudomonas aeruginosa and Staphylococcus aureus*. Lett Appl Microbiol 48(2):173–179
23. Li WR, Xie XB, Shi QS, Duan SS, Ouyang YS, Chen YB (2011) Antibacterial effect of silver nanoparticles on *Staphylococcus aureus*. Biometals 24(1):135–141
24. de Azeredo HMC (2013) Antimicrobial nanostructures in food packaging. Trends Food Sci Technol 30(1):56–69
25. Cushen M, Kerry J, Morris M, Cruz-Romero M, Cummins E (2012) Nanotechnologies in the food industry e recent developments, risks and regulation. Trends Food Sci Technol 24(1):30–46
26. Llorens A, Lloret E, Picouet P, Fernandez A (2012) Study of the antifungal potential of novel cellulose/copper composites as absorbent materials for fruit juices. Int J Food Microbiol 158(2):113–119
27. Muthulakshmi L, Rajini N, Varada Rajulu A, Siengchin S, Kathiresan T (2017) Synthesis and characterization of cellulose/silver nanocomposites from bioflocculant reducing agent. Int J Biol Macromol 103:1113–1120
28. Bagul M, Sonawane SK, Arya SS (2015) Tamarind seeds: chemistry, technology, applications and health benefits: a review. Indian Food Ind Mag 34(3):28–35
29. Xu CS, Tian CC, Zhang WD, Xing JW, Cai ZS, Ren Y, Xu WZ, Liu HZ (2014) Synthesis and properties of polypropylene carbonate polyol-based waterborne polyurethane. Adv Mater Res 936:58–62
30. Zheng F, Mi QH, Zhang K, Xu J (2016) Synthesis and characterization of poly(propylene carbonate)/ modified sepiolite nanocomposites. Polym Compos 37(1):21–27
31. Gopinath V, Mubarak Ali D, Priyadarshini S, Meera Priyadharsshini N, Thajuddin N, Velusamy P (2012) Biosynthesis of silver nanoparticles from *Tribulus terrestris* and antimicrobial activity: a novel biological approach. Colloids Surf B 96:69–74
32. Basavegowda N, Idhayadhulla A, Lee YR (2014) Preparation of Au and Ag nanoparticles using *Artemisia annua* and their in vitro antibacterial and tyrosinase inhibitory activities. Mater Sci Eng C 43:56–64
33. Bindhu MR, Umadevi M (2013) Synthesis of monodispersed silver nanoparticles using *Hibiscus cannabinus* leaf extract and its antimicrobial activity. Spectrochim Acta A 101:184–190
34. Suvith VS, Philip D (2014) Catalytic degradation of methylene blue using biosynthesized gold and silver nanoparticles. Spectrochim Acta A 118:526–532
35. Kumar V, Yadav SK (2009) Plant mediated synthesis of silver and gold nanoparticles and their applications. J Chem Technol Biotechnol 84:151–157
36. Jeeva K, Thiyagarajan M, Elangovan V, Geetha N, Venkatachalam P (2014) *Caesalpinia coriaria* leaf extracts mediated biosynthesis of metallic silver nanoparticles and their antibacterial activity against clinically isolated pathogens. Ind Crop Prod 52:714–720
37. Aseer JR, Sankaranarayanasamy K (2017) Effect of fiber content on tensile retention properties of cellulose microfiber reinforced polymer composites for automobile application. IOP Con Ser-Mat Sci 272:012020
38. Senthil Muthu Kumar T, Rajini N, Jawaid M, Rajulu AV, Jappes JTW (2018) Preparation and properties of cellulose/tamarind nut powder green composites. J Nat Fibers 15(1):11–20
39. Petrosino JF, Galhardo RS, Morales LD, Rosenberg SM (2009) Stress-induced beta-lactam antibiotic resistance mutation and sequences of stationary-phase mutations in the *Escherichia coli* chromosome. J Bacteriol 191(19):5881–5889
40. Webber MA, Piddock LJV (2002) The importance of efflux pumps in bacterial antibiotic resistance. J Antimicrob Chemother 51(1):9–11
41. Nikaido H (2009) Multidrug resistance in Bacteria. Annu Rev Biochem 78:119–146
42. Paramasivam P, Mudili V, Marriappan A, Periyasamy V, Kadirvelu K, Ramasamy R (2015) Biological synthesis and characterization of silver nanoparticles using *Eclipta alba* leaf extract and evaluation of its cytotoxic and antimicrobial potential. Bull Mater Sci 38(4):965–973
43. Ajitha B, Reddy AKY, Reddy SP (2014) Biogenic nano-scale silver particles by Tephrosia purpurea leaf extract and their inborn antimicrobial activity. Spectrochim Acta A 121:164–172